Coherent spin dynamics in gadolinium-doped CaWO4 crystal

E I Baibekov, M R Gafurov, D G Zverev, I N Kurkin, A A Rodionov, B. Z Malkin, B. Barbara

Coherent spin dynamics in gadolinium-doped $CaWO_4$ crystal

E. I. Baibekov[a,*], M. R. Gafurov[a], D. G. Zverev[a], I. N. Kurkin[a], A. A. Rodionov[a],
B.Z. Malkin[a], B. Barbara[b]

[a] *Kazan Fedral University, 420008 Kazan, Russia*

[b] *Institut Néel, CNRS, BP166, 38042 Grenoble Cedex 9*

and Université Joseph Fourier, France

*Corresponding author. E-mail address: edbaibek@gmail.com

Abstract

We report the first observation of Rabi oscillations in the spin-7/2 ensemble of trivalent gadolinium ions hosted in $CaWO_4$ single crystal. A number of transitions within the lowest electronic multiplet ${}^8S_{7/2}$ of Gd^{3+} ion are studied using a combination of continuous-wave and pulsed electron paramagnetic resonance spectroscopy. The corresponding Rabi damping curves and the spin coherence times are detected at varying strengths of the microwave field. These data are well reproduced by a theoretical model which accounts for the inhomogeneity of the microwave field within the crystal sample volume and the magnetic dipole interactions in the diluted spin ensemble.

Keywords: Rabi Oscillations; Transient Nutations; Quantum Coherence; Electron Paramagnetic Resonance; Gadolinium; Calcium Tungstate

1. Introduction

The concept of bulk quantum computing (QC) implies that the same computation algorithm is executed simultaneously within a large number of identical noninteracting spin systems [1]. The spin states are addressed by means of conventional methods of pulsed magnetic resonance spectroscopy. A simple transient pulse with frequency matching that of a certain quantum transition can be viewed as one-qubit gate [2]. For example, a π pulse flipping the spin-1/2 states represents quantum NOT gate. One clear advantage of this scheme is that it provides the grounds for testing the basic concepts of QC with no specific instrumentation apart from commercial nuclear magnetic

resonance (NMR) or electron paramagnetic resonance (EPR) spectrometer. In particular, implementation of 7-qubit Shor's factoring algorithm using the nuclear spin states of perfluorobutadienyl iron complex culminated the first rapid progress of NMR quantum computation in the early 2000s [3]. A thorough theoretical analysis, however, showed that the sole use of nuclear spin states with achievable population difference $< 10^{-3}$ actually provided no quantum entanglement and restrained the scalability of the NMR quantum computer [4,5]. On the contrary, typical X-band EPR provides sufficient pure component of an electron spin density matrix at temperatures ~ 1 K to overcome aforementioned issues. In the case of EPR QC, the following problems arise:

(i) The electron spin coherence times are usually much shorter than the nuclear ones. The number of coherent QC operations is much smaller, even considering the difference in the excitation frequency.

(ii) The possibility to excite different transitions during the NMR pulse sequence was a key capability that induced the first success of multiqubit NMR QC. Up to the moment, no commercialized EPR instrumentation allows complete control over the pulse shape and frequency, with a possible exception of Bruker SpinJet-AWG system [6]. Two-qubit electronic or hybrid electron-nuclear systems can be operated by pulsed electron-electron (ELDOR) or electron-nuclear (ENDOR) double resonance techniques, respectively [7].

The best-known implementations of solid-state EPR QC include: NV-centers in diamond [8], single-molecule magnets [9], organic radicals [7], rare earth and transition metal ions in crystals [10]. Most of these quantum systems have rich energy level structure, although large difference in the excitation frequencies complicates the selective excitation of various quantum transitions during the pulse sequence. It is well-known that the lowest states of ions with half-filled valence shell, so-called S-state ions (Fe^{3+}, Mn^{2+}, Gd^{3+}, Eu^{2+}, ...) are characterized by certain total spin S and zero total orbital moment, so that spin-lattice and crystal-field interactions are effectively suppressed [11]. These ions can be actually treated as particles bearing large spin S. Zeeman interaction creates nearly equidistant lower energy level scheme. Rabi oscillations (ROs) of Mn^{2+} ions ($S = 5/2$) in MgO crystal have been studied recently [12,13]. S-state lanthanide ions (Eu^{2+}, Gd^{3+}, Tb^{4+}) have more complex energy level scheme and larger number of observable transitions due to higher spin $S = 7/2$. To the best of our knowledge, no demonstration of coherent spin dynamics of the S-state lanthanide ions has ever been published. In the present article, we fill this gap by providing the first experimental evidence of collective spin nutations in the ensemble of trivalent gadolinium ions incorporated in $CaWO_4$ single crystal.

2. Experimental procedure

The sample of $CaWO_4:Gd^{3+}$ single crystal was grown by Czochralski method in Magnetic Resonance Laboratory of Kazan State University. Nominal concentration of gadolinium ions equaled 0.01 at. % ($C = 1.28 \cdot 10^{18}$ ions per cc.), which was verified within relative error of 20% by comparative measurements of continuous-wave (cw) EPR spectral intensities with respect to the reference sample of $LiYF_4:Gd^{3+}$ with known concentration of 0.5 at. %. In order to reduce the effect of microwave (mw) field inhomogeneity on the Rabi decay times, a small plate with approximate dimensions $2 \times 3 \times 0.5$ mm was cut from the original sample. A quartz tube containing this smaller sample was placed close to the center of standard cylindrical dielectric resonator Bruker EN 4118X-MD4 of X-band Elexsys 580/680 EPR spectrometer. Parallel orientation of the crystal sample axis *c* with respect to the static magnetic field $\boldsymbol{B}_0$ (see Fig. 1) was checked by comparison of the calculated and measured cw EPR spectra.

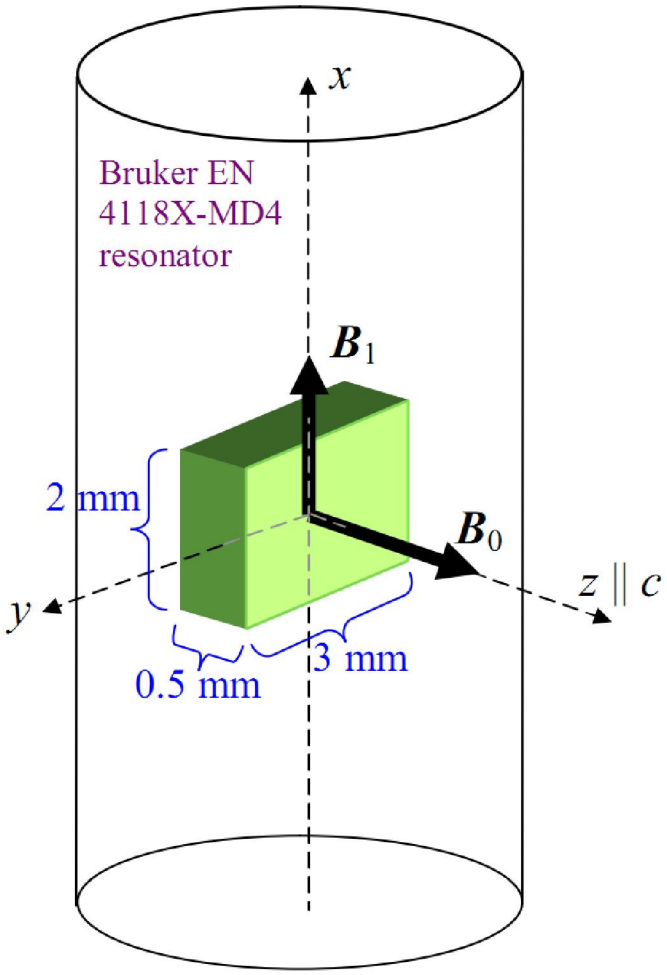

Fig. 1. (Color online) A scheme that represents the orientation of the crystal sample of $CaWO_4:Gd^{3+}$ with respect to the resonator axis, static and mw field vectors $\boldsymbol{B}_0$ and $\boldsymbol{B}_1$.

Room-temperature cw EPR spectra were acquired at $\omega_0/2\pi = 9.66$ GHz and in the field range of $\boldsymbol{B}_0 = 0 \div 10000$ G. Due to the presence of spin-lattice relaxation, pulsed measurements were accomplished in the temperature range $T = 6$-15 K. Spin-lattice relaxation times T_1 and phase memory times T_2 were acquired by means of inversion-recovery ($\pi - \tau - \pi/2 - \tau' - \pi$) and Hahn spin echo ($\pi/2 - \tau - \pi$) pulse sequences, respectively, where τ was incremented and τ' kept constant. Each data point of ROs was obtained as a result of the pulse sequence shown in Fig. 2, where the transient pulse of length t was followed by the spin-echo detection sequence. The durations of $\pi/2$ and π pulses above equaled 8 and 16 ns, respectively. After that, the sequence was repeated with time t incremented by 4 ns. As a result, we obtained time dependence of the longitudinal magnetic moment $M_Z(t)$ of the Gd^{3+} ($S = 7/2$) spin ensemble in the form of the decaying oscillations. The frequency of the oscillations (Rabi frequency) Ω_R was proportional to the mw field amplitude B_1, or to the square root of the mw field attenuation.

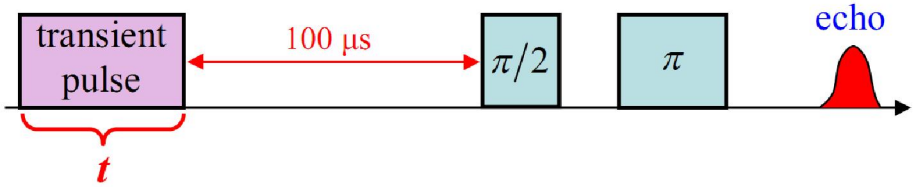

Fig. 2. (Color online) Transient pulse sequence that was applied in order to record ROs of Gd^{3+} ions in $CaWO_4$ crystal. The duration of $\pi/2$ and π pulses equaled 8 and 16 ns, respectively. The time t was varied from 0 to 2 μs with a step of 4 ns.

A tiny coal sample was used to calibrate the distribution $\boldsymbol{B}_1(x)$ along the resonator axis. The relative amplitudes $B_1(x)/B_1^{(\max)}$ were determined by comparing the cw EPR signals at different positions of a sample tube with respect to the field antinode of the resonator (Fig. 3).

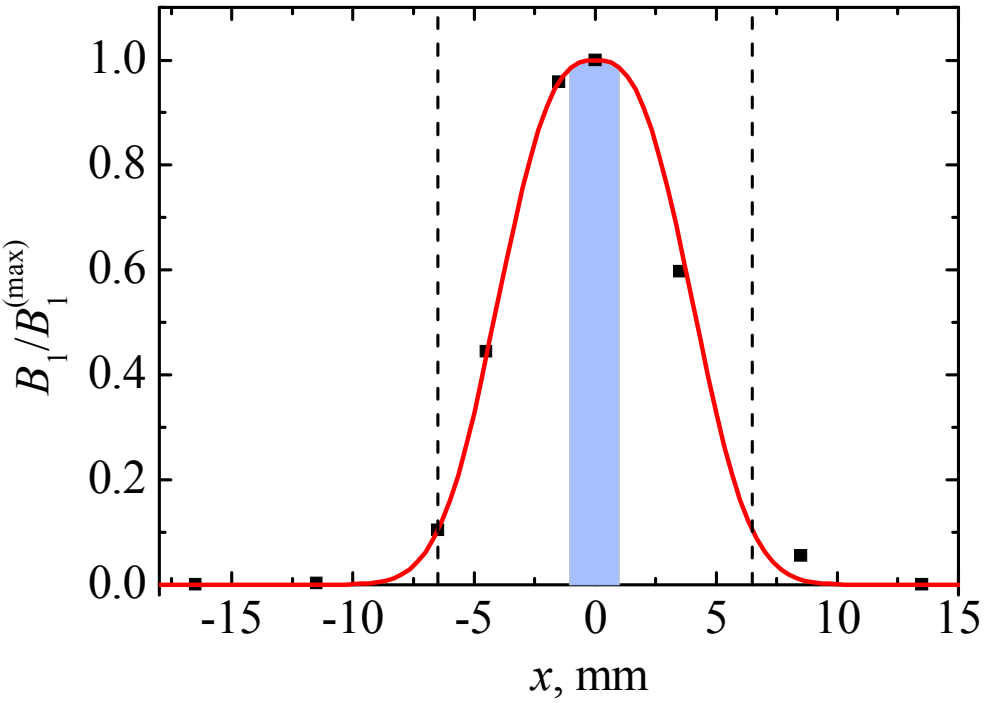

Fig. 3. (Color online) The distribution of the mw field amplitude along the resonator axis. Experimental data and their fit by the generalized Gaussian distribution function $\exp\left[-(x/a)^b\right]$ ($a = 4.8$ mm, $b = 2.7$) are represented by the black squares and the red line, respectively. A blue fill area corresponds to the approximate position occupied by the crystal sample of $CaWO_4:Gd^{3+}$.Vertical dashed lines show the borders of the 13 mm-long resonator.

3. Results and discussion

The cw EPR spectra of Gd^{3+} ions in various host crystals [14], particularly in $CaWO_4$ single crystal [15-19], had been extensively studied. The present-work cw EPR spectra recorded at $\boldsymbol{B}_0 \parallel c$ are shown in the top part of Fig. 4. There, ca. 17 electron spin transitions $M_1 \leftrightarrow M_2$ ($M_i = -7/2 \ldots 7/2$) were identified by means of the numerical diagonalization of the spin Hamiltonian containing Zeeman and crystal-field interactions,

$$H = g_{\parallel}\mu_B S_Z B_0 + B_2^0 O_2^0 + B_4^0 O_4^0 + B_4^4 O_4^4 + B_6^0 O_6^0 + B_6^4 O_6^4, \qquad (1)$$

where O_p^k are Stevens operators constructed on the basis of 8 spin-7/2 states ($^8S_{7/2}$ multiplet), μ_B is Bohr magneton. The g-factors $g_{\parallel} = 1.991$, $g_{\perp} = 1.992$ and the crystal field parameters (in units of cm^{-1}) $B_2^0 = -0.0298$, $B_4^0 = -3.80 \cdot 10^{-5}$, $B_4^4 = -2.34 \cdot 10^{-4}$, $B_6^0 = 1.98 \cdot 10^{-8}$, $B_6^4 = 1.59 \cdot 10^{-8}$ had been determined previously [16]. The calculated energies of the $^8S_{7/2}$ electronic levels versus magnetic field are presented on the bottom part of Fig. 4. Numerically calculated EPR spectra (not shown)

were in good agreement with the experimental data. The observed transitions were classified as follows:

(i) The most intense were $M \leftrightarrow M \pm 1$ transitions excited by the interaction with the mw field $H_{MW} = 2g_{\perp}S_X B_1 \cos\omega_0 t$ (shown in Fig. 4 by green arrows).

(ii) The tetragonal-symmetry crystal field interaction mixed M and $M \pm 4$ states, which resulted in lower-intensity $M \leftrightarrow M \pm 3$ and $M \leftrightarrow M \pm 5$ transitions (blue arrows).

(iii) The smallest signals came from the forbidden transitions $M \leftrightarrow M \pm 2$ and $M \leftrightarrow M \pm 4$ (red arrows). The necessary mixing of the states $M \leftrightarrow M \pm 1$, $M \leftrightarrow M \pm 3$ presumably originated from the presence of nearby crystal lattice defects lowering the tetragonal symmetry, and/or hyperfine interactions with ^{155}Gd and ^{157}Gd nuclei.

One can identify at least four field regions (near 660, 1780, 2670 and 5000 G, see brown rectangles on the lower part of Fig. 4), where two and more transitions connecting at least three energy levels fall into the frequency band of 9.6 ± 0.5 GHz accessible by the pulsed ELDOR techniques. For instance, at $B_0 = 2670$ G, a subgroup of four electronic states can be manipulated through the transitions $7/2 \leftrightarrow -3/2$, $7/2 \leftrightarrow 1/2$ and $7/2 \leftrightarrow 5/2$ within the frequency bandwidth of ~ 1 GHz.

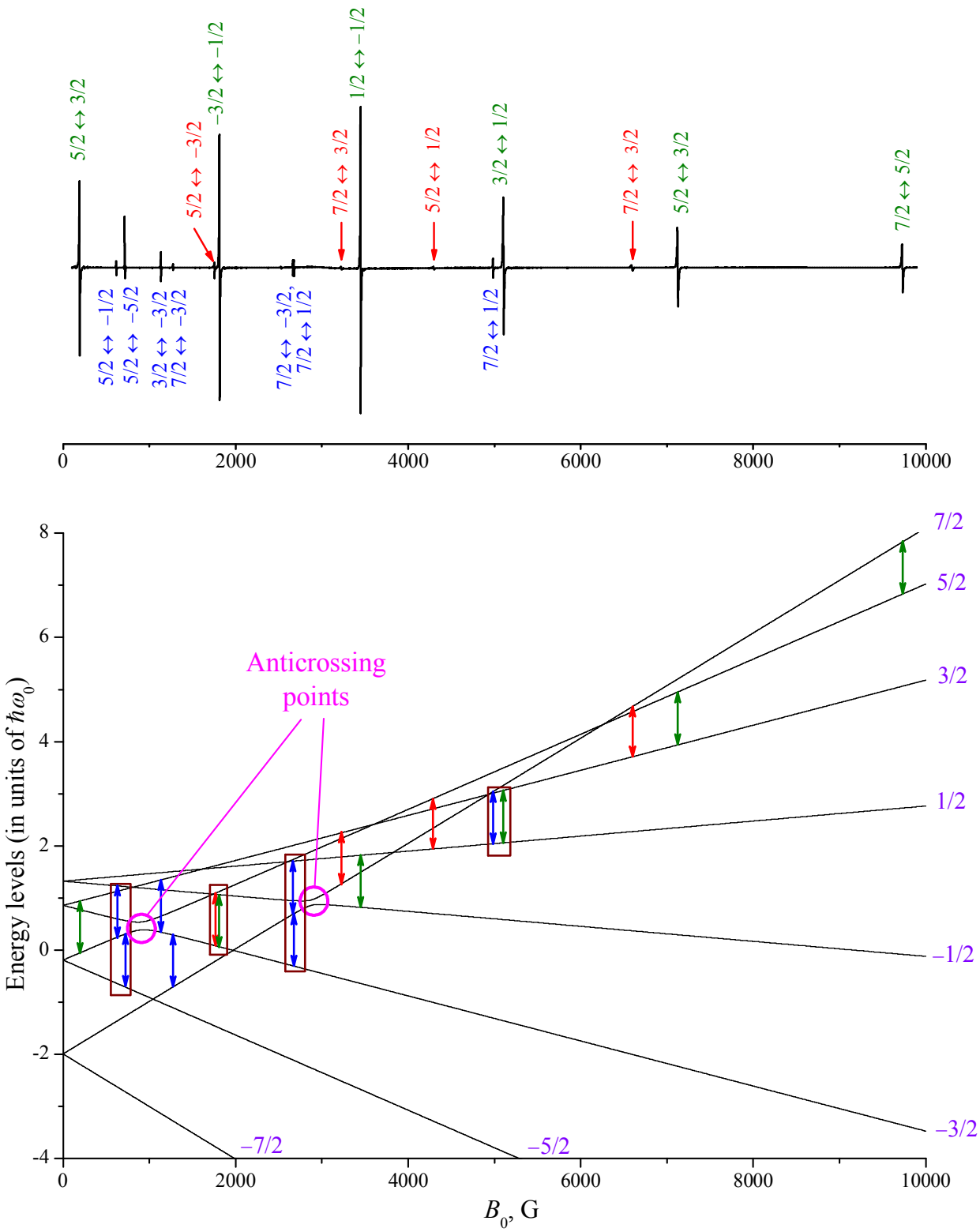

Fig. 4. (Color online) X-band EPR spectra of Gd^{3+} ion in $CaWO_4$ crystal (top), and the calculated energy levels of the lowest ${}^8S_{7/2}$ multiplet versus magnetic field (bottom). $T = 300$ K, $\omega_0/2\pi = 9.66$ GHz. Different transitions are marked with green, blue and red arrows, see text. Two anticrossing points that arise from mixing of $5/2 \leftrightarrow -3/2$ and $7/2 \leftrightarrow -1/2$ spin levels by the $B_4^4 O_4^4$, $B_6^4 O_6^4$ terms of the crystal field interaction are marked with pink circles. Brown rectangles show regions containing multiple transitions accessible by the pulsed ELDOR.

Due to narrower EPR lines at low temperatures, an observation of the hyperfine structure was sometimes possible. Field-swept echo-detected spectrum near the $1/2 \leftrightarrow -1/2$ electronic transition with full width at half-maximum (FWHM) ~ 2.5 G at 15 K revealed the presence of ^{155}Gd and ^{157}Gd isotopes with the nuclear spin $I = 3/2$ (natural abundance 14.7 % and 15.7 %, respectively), see Fig. 5. The positions of the hyperfine components agree well with the previously reported hyperfine constants $A_{155} = 12.40$ and $A_{157} = 16.28$ MHz [15].

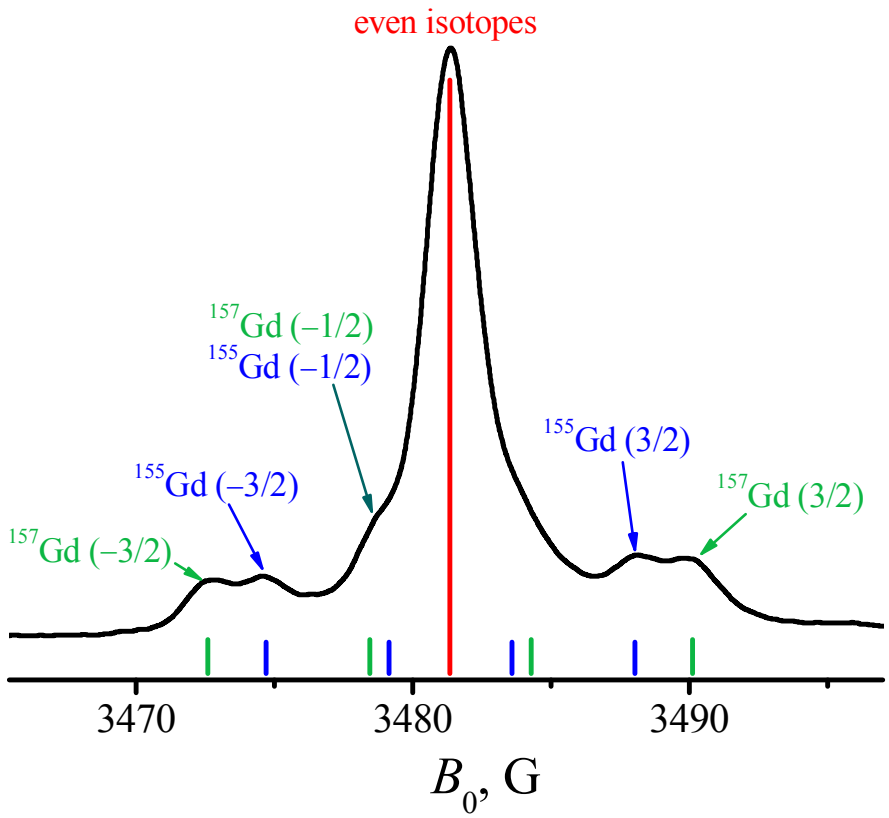

Fig. 5. (Color online) Field-swept echo-detected EPR spectrum near the $1/2 \leftrightarrow -1/2$ electronic transition revealing the hyperfine structure due to the presence of ^{155}Gd and ^{157}Gd isotopes (nuclear spin 3/2). The bars show the calculated positions of the hyperfine lines with respect to the central line and their relative intensities. $T = 15$ K, $\omega_0/2\pi = 9.75$ GHz.

The T_2 and T_1 times corresponding to the intense $M \leftrightarrow M \pm 1$ transitions were measured at 6 and 15 K. The results are presented in the last two columns of Table 1. Our experimental T_1 values ~ 8 ms at 6 K and ~ 1 ms at 15 K are comparable to the previously reported data acquired by the pulse saturation technique [20]. The corresponding T_2 times of ~ 5÷10 μs depended on temperature, which indicated the possible impact of the spectral diffusion process associated with the spin-lattice relaxation of the surrounding spins [21]. Nearly two times longer T_2 values in the case when the magnetic field $B_0 = 3473$ G was tuned to the $m_I = -3/2$ hyperfine component of the

^{157}Gd $1/2 \leftrightarrow -1/2$ transition suggested that the dominant contribution came from the instantaneous diffusion process [22]. This suggestion was also corroborated by the observation of sufficiently longer T_2 times upon 10-time increase of the $\pi/2$ and π pulse duration. Due to negligible amount of the magnetic ^{43}Ca and ^{183}W isotopes, and the gadolinium dilution sufficient enough to rule out the exchange interactions, the experimental T_2 values were simulated taking into account only the magnetic dipole interactions between the Gd^{3+} ions:

$$T_2^{(\mathrm{Th})} = \left(\Gamma_{\mathrm{ID}} + \Gamma_{\mathrm{SD}}\right)^{-1}. \tag{2}$$

Above, Γ_{ID} is the rate of the instantaneous diffusion process associated with the change of the local magnetic field induced by the flipping nearby gadolinium spins at the application of the second (π) pulse of the spin-echo sequence [22]. This rate was estimated as

$$\Gamma_{\mathrm{ID}} = \gamma_T \Delta\omega_d \left\langle \sin^2 \frac{\theta_\pi}{2} \right\rangle, \tag{3}$$

where $\Delta\omega_d = 4\pi^2 g_\parallel^2 \mu_B^2 C / 3\sqrt{3}\hbar = 1.05 \cdot 10^6$ s^{-1} is the dipolar half-width of the EPR line calculated for the diluted ensemble of the spin-1/2 particles [21,23] (for the $M \leftrightarrow M+1$ transition, π pulse changed the spin projection by unity, thus the change of the local field was equivalent to the one in the spin-1/2 ensemble); θ_π is the angle by which the π pulse rotates a given spin packet, $\langle \ldots \rangle$ denotes averaging over all spin packets within the line of spectral density $g(\omega)$; $\left\langle \sin^2 \theta_\pi/2 \right\rangle$ was calculated according to the Ref. [22] as

$$\left\langle \sin^2 \frac{\theta_\pi}{2} \right\rangle = \int d\omega g(\omega) \frac{\Omega_R^2}{(\omega - \omega_0)^2 + \Omega_R^2} \sin^2 \left\{ \frac{\pi}{2} \left[\frac{(\omega - \omega_0)^2}{\Omega_R^2} + 1 \right] \right\}. \tag{4}$$

The Rabi frequency $\Omega_R/2\pi = 1/(2t_\pi)$ equaled 31.2 MHz in the case of the $t_\pi = 16$ ns π-pulse duration. The above integral was calculated numerically for all studied transitions, where $g(\omega)$ were acquired directly from the field-swept echo-detected EPR spectra, which showed combinations of nearly Lorentzian lines with FWHM varying in the range of ~ 2.5÷16 G (see Fig. 5 and the 3$^{\mathrm{rd}}$ column of the Table 1). At $t_\pi = 16$ ns, we obtained $\left\langle \sin^2 \theta_\pi/2 \right\rangle$ ~ 0.7-0.8, meaning that the most part of the spin packets were excited by the spin-echo sequence. At $t_\pi = 160$ ns and for the hyperfine ^{157}Gd transition, $\left\langle \sin^2 \theta_\pi/2 \right\rangle$ ~ 0.04, which explained longer T_2 ~ 25 μs.

The temperature factor γ_T was added into Eq. (3) to account for only those spins that populate the M and $M+1$ levels involved in the transition (with the corresponding energies E_M and E_{M+1})

$$\gamma_T = \frac{\exp\left(-E_M/k_BT\right)+\exp\left(-E_{M+1}/k_BT\right)}{\sum_{M'=-S}^{S}\exp\left(-E_{M'}/k_BT\right)}. \tag{5}$$

At infinite temperature, $\gamma_\infty = 0.25$. It can differ considerably from 0.25 at 6K, giving longer T_2 times ~ 10 μs for the high-field $5/2 \leftrightarrow 3/2$ and $7/2 \leftrightarrow 5/2$ transitions.

The second studied mechanism was the spectral diffusion [21,22], in which the local fields were fluctuated by spontaneous flips of the nearby spins induced by the spin-lattice and by the magnetic dipole interactions. The latter, however, were negligible since the dipolar-induced flip-flop processes are unfavorable when $\Delta\omega_d \ll$ FWHM, i.e. when the lines are inhomogeneously broadened. The rate of the spectral diffusion was calculated as follows

$$\Gamma_{\mathrm{SD}} = \sqrt{f_S \Delta\omega_d \tilde{T}_1^{-1}/2}\,, \tag{6}$$

where the factor $f_S \sim 3$ was added to $\Delta\omega_d$ in order to account for the random $M' \to M''$ flips with $|M'-M''|>1$ ($f_S = 1$ for $S = 1/2$), and $\tilde{T}_1^{-1}$ was the flip rate averaged over all transitions at a given temperature (on the basis of our experimental T_1 values, we chose $\tilde{T}_1 = 8$ ms at 6 K and $\tilde{T}_1 = 1$ ms at 15 K). According to our calculations, instantaneous diffusion prevailed over the spectral diffusion. Only in the case of longer pulses and/or hyperfine transitions the contribution of the latter was significant. One can see in Table 1 that the calculated $T_2^{(\mathrm{Th})}$ are in reasonable agreement with the experimental T_2 values.

Table 1

The phase memory (T_2) and the spin-lattice relaxation (T_1) times measured at 6 and 15 K for various quantum transitions. $\omega_0/2\pi = 9.75$ GHz. The calculated phase memory time $T_2^{(\mathrm{Th})}$, see Eq. (2), contained the contributions from the instantaneous (Γ_{ID}) and spectral (Γ_{SD}) diffusion mechanisms.

B_0, G (transition)	T, K	FWHM, G	Γ_{ID}, 10^5 s^{-1}	Γ_{SD}, 10^5 s^{-1}	$T_2^{(\mathrm{Th})}$, μs	T_2, μs	T_1, ms
1806 ($-3/2 \leftrightarrow -1/2$)	6	2.7	1.8	0.14	5.1	5.4	8
	15		1.9	0.40	4.3	5.1	0.97
3482 ($1/2 \leftrightarrow -1/2$)	6	2.5	1.9 1.1[a] 0.69[b] 0.09[ab]	0.14 0.14[a] 0.14[b] 0.14[ab]	4.8 7.8 12 44	6.5 10.2[a] 12[b] 25[ab]	8 6[a] 2.6[b] 3.5[ab]
	15		2.1 1.2[a] 0.09[ab]	0.40 0.40[a] 0.40[ab]	4.0 6.1 20	5.4 8.9[a] 13.1[ab]	1.2 1.15[a]
5178 ($3/2 \leftrightarrow 1/2$)	6	10	1.4	0.14	6.4	6.4	7
	15		1.6	0.40	4.8	5.3	0.9
7240 ($5/2 \leftrightarrow 3/2$)	6	13	1.2	0.14	7.4	8.6	7
	15	16	1.5	0.40	5.2	5.4	0.8
9892 ($7/2 \leftrightarrow 5/2$)	6	15	0.94	0.14	9.2	13.1	10
	15		1.5	0.40	5.2	10.6	0.85

[a] the data are presented for $m_I = -3/2$ transition of the ^{157}Gd isotope ($B_0 = 3473$ G)

[b] the durations of $\pi/2$ and π pulses were 10 times longer (80 and 160 ns, respectively)

ROs corresponding to all studied $M \leftrightarrow M \pm 1$ transitions were acquired, some of them are presented in Figs. 6 and 7. The Rabi frequences $\Omega_R/2\pi \sim$ 28÷33 MHz were determined from the observed $M_Z(t)$ dependences. Up to 80 Rabi half-periods were observed, each corresponding to one-qubit NOT gate. The Rabi time τ_R (damping time of ROs) was roughly proportional to Ω_R^{-1}. The resulting decay profiles were found almost independent of the transition filed, gadolinium isotope and temperature. The damping was essentially slower than exponential. These facts ruled out the dipolar origin of the Rabi damping and suggested that the greatest contribution came from the distribution of the mw field $\boldsymbol{B}_1(\boldsymbol{r})$ within the sample volume. The experimental data were successfully simulated by the following expression:

$$M_Z(t) \sim \int_V d\boldsymbol{r} \int g(\omega) d\omega \frac{\cos\left(\sqrt{\Omega_R^2(\boldsymbol{r}) + (\omega - \omega_0)^2} \cdot t\right)}{\Omega_R^2(\boldsymbol{r}) + (\omega - \omega_0)^2} \times \exp(-\Gamma_d t). \qquad (7)$$

Here $\sqrt{\Omega_R^2(\boldsymbol{r}) + (\omega - \omega_0)^2}$ is the nutation frequency of the spin packet detuned by $\omega - \omega_0$ from the resonant frequency, $\Omega_R(\boldsymbol{r}) = g_\perp \mu_B B_1(\boldsymbol{r})/\hbar$ corresponds to the local Rabi frequency of the

spin-bearing particle situated at the site $\boldsymbol{r}$ within the crystal sample, $\boldsymbol{r}=0$ corresponds to the field antinode, and $\Omega_R=\Omega_R\left(\boldsymbol{r}=0\right)$ is related to the most "coherent" part of the spin ensemble. The integration over the sample volume V was performed numerically, using the measured distribution of the mw field amplitude along the resonator axis $B_1\left(x\right)$ (Fig. 3), and admitting simple Gaussian distribution $\sim \exp\left[-\left(y^2+z^2\right)/c^2\right]$ in perpendicular plane with $c=4.3$ mm. That corresponded to the maximum inhomogeneity of ~ 13 % within the sample volume, i.e. $0.87\Omega_R \le \Omega_R\left(\boldsymbol{r}\right) \le \Omega_R$. The amplitude of ROs had polynomial decay $\sim \left[1+\left(t/\tau_R\right)\right]^{-n}$, and was modulated due to the constructive/destructive interference of the nutations from the different areas of the sample [24,25].

The exponential factor in Eq. (7) accounts for the magnetic dipole interactions between the spins. In analogy with the instantaneous diffusion process, only those spins that are driven by the mw field contribute to the local magnetic field and influence the decay time [26]. In the present case of narrow line broadening (FWHM < $2\Omega_R$), the decay rate was approximately a half of the dipolar half-width multiplied by the temperature factor γ_T, cf. Eq. (3) (a comprehensive analysis of the $\Gamma_d\left(C,\Omega_R,\mathrm{FWHM}\right)$ dependence was presented in Ref. [26]):

$$\Gamma_d \approx \frac{1}{2}\gamma_T \Delta\omega_d \,. \tag{8}$$

Our estimations give rather long dipolar relaxation times $\Gamma_d^{-1} \sim 8$ μs $\gg \tau_R$. Thus, the role of the dipolar coupling was rather small in comparison with the spin dephasing caused by the spatial inhomogeneity of the mw field. The results of calculations agree well with the experimental data, see Fig. 7. In the case when the field inhomogeneity is eliminated, for the same Ω_R, one can expect the damping times of ~ 8 μs, which correspond to ~ 500 one-qubit operations. This can be achieved by using smaller samples (however, at the sacrifice of the signal-to-noise ratio), or utilizing the rotation angle correction schemes like the BB1 composite pulse sequence [27-29].

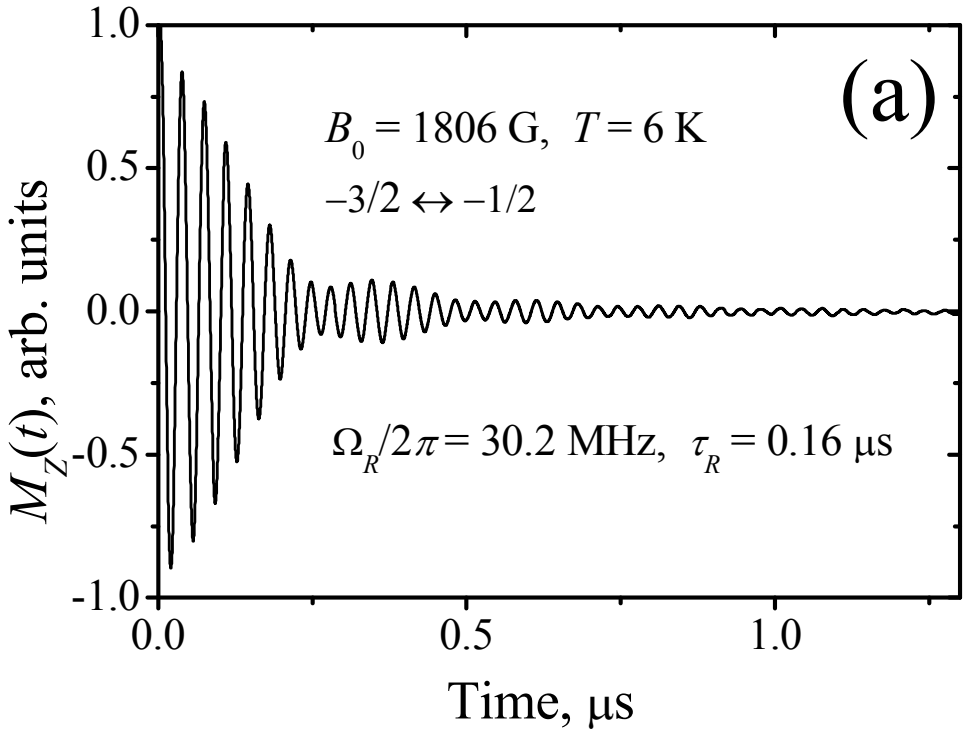
(a)
B_0 = 1806 G, T = 6 K
−3/2 ↔ −1/2
$\Omega_R/2\pi$ = 30.2 MHz, τ_R = 0.16 μs
$M_Z(t)$, arb. units
Time, μs
1.0
0.5
0.0
-0.5
-1.0
0.0
0.5
1.0

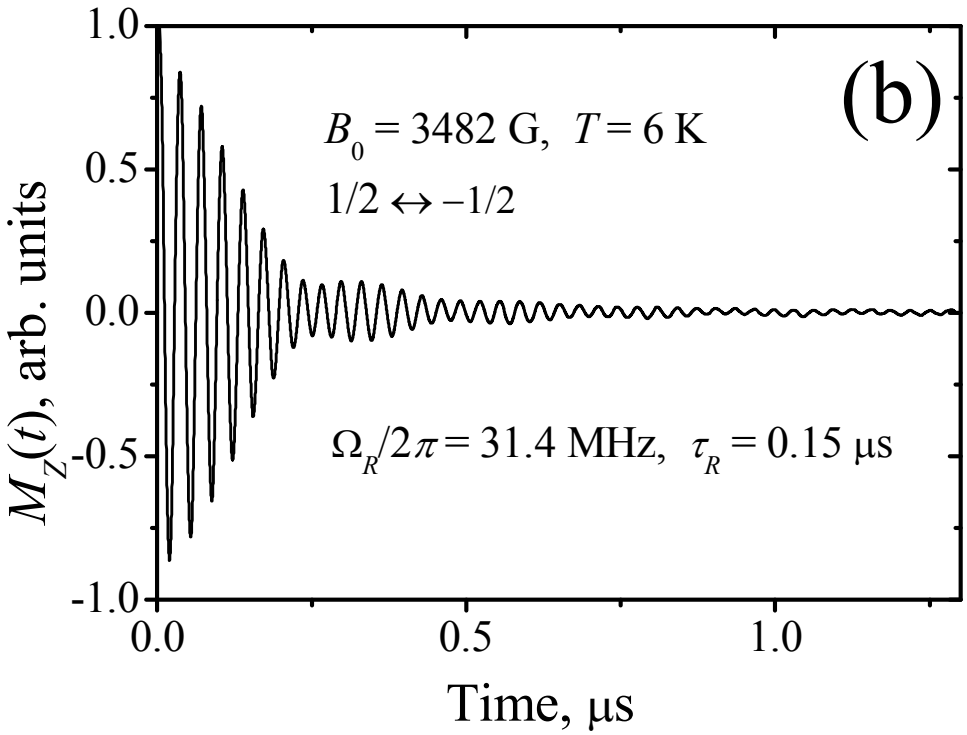
(b)
B_0 = 3482 G, T = 6 K
1/2 ↔ −1/2
$\Omega_R/2\pi$ = 31.4 MHz, τ_R = 0.15 μs
$M_Z(t)$, arb. units
Time, μs
1.0
0.5
0.0
-0.5
-1.0
0.0
0.5
1.0

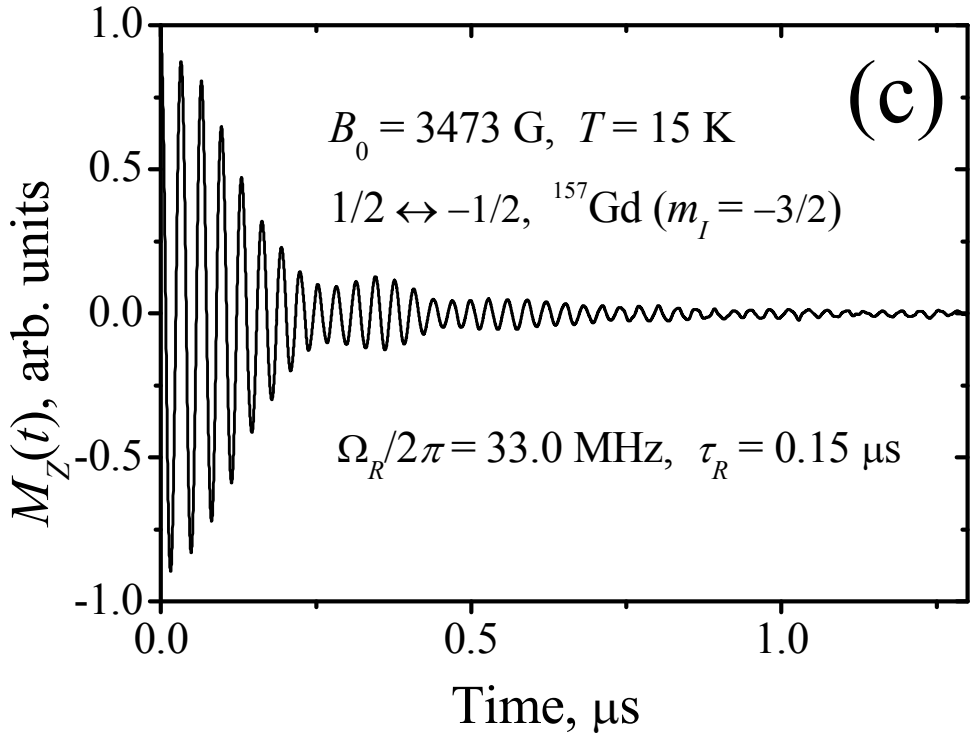

Fig. 6. Rabi oscillations between the quantum states of the spin-7/2 trivalent gadolinium ion in $CaWO_4$ crystal. The level notations are the same as in Figs. 4 and 5. Rabi frequencies $\Omega_R/2\pi$ and Rabi times τ_R were determined from these experimental data as the frequencies of the damped oscillations and the characteristic damping times, respectively. $\omega_0/2\pi = 9.75$ GHz.

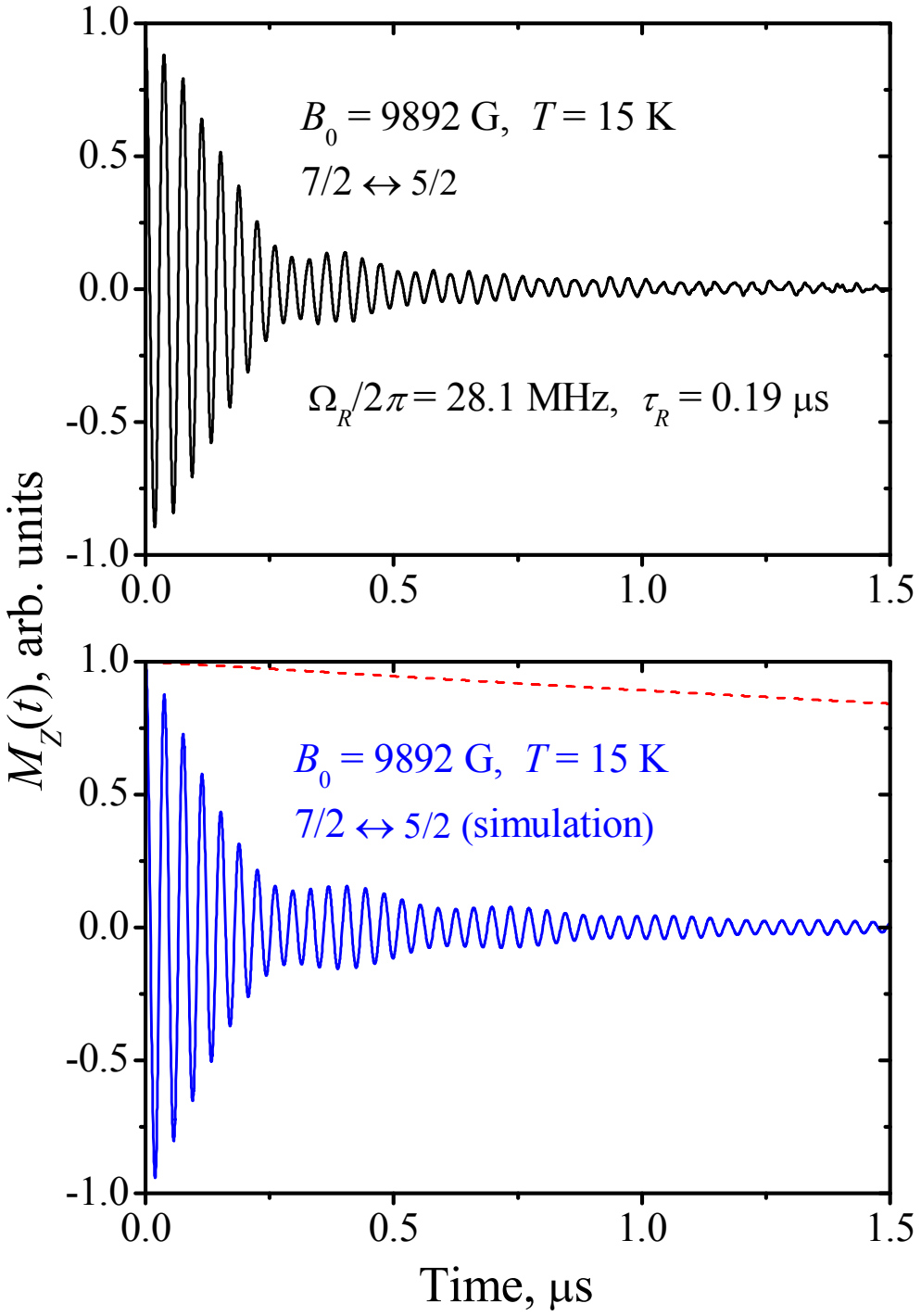

Fig. 7. (Color online) Rabi oscillations of the $7/2 \leftrightarrow 5/2$ transition at 9892 G. The experimental data and the calculations of the total magnetic moment according to the Eq. (7) are shown by the black (top) and blue (bottom) solid lines, respectively. The red dashed line is the calculated amplitude of the damped oscillations in the case when the inhomogeneity of the mw field within the sample is totally compensated.

4. Conclusions

In the present article, coherent manipulations of the quantum states belonging to the spin-7/2 trivalent gadolinium ion are implemented for the first time. Coherence times and Rabi oscillations were acquired at different lines of fine and hyperfine structure of the Gd^{3+} ion hosted in $CaWO_4$ single crystal. Spin-lattice relaxation times up to 8 ms and phase memory times up to 25 μs were recorded in the temperature interval 6-15 K. The Rabi damping times and the phase memory times were interpreted in the framework of a model that takes into account the magnetic dipole interactions between the ions and, in the case of the Rabi damping, the intrinsic inhomogeneity of the microwave field inside the resonator.

The observed rich level structure of the S-state Gd^{3+} ion in $CaWO_4$ crystal provides the opportunity to tune the microwave frequency, the magnetic field and the sample orientation in order to apply appropriate quantum computation scheme. We experimentally demonstrated the possibility to perform up to 80 coherent one-qubit operations on various X-band EPR transitions of the lowest electronic ${}^8S_{7/2}$ multiplet (this figure can be potentially increased to ~ 500). In comparison with the previously studied spin-5/2 Mn^{2+} ion [12,13], the present system offers somewhat larger Hilbert space of $8 = 2^3$ addressable quantum states, meaning that each Gd^{3+} ion can represent three effective qubits. Moreover, $^{155}Gd^{3+}$ and $^{157}Gd^{3+}$ ions with nuclear spin $I = 3/2$ are potential hybrid 5-qubit systems, whose states can be accessed via pulsed ENDOR.

Acknowledgement

EIB was funded by the Russian President Fellowship for Young Scientists (stipend no. 924.2015.5).

References

[1] N. Gershenfeld, I. L. Chuang, Bulk spin-resonance quantum computation, Science 275 (1997) 350-356.

[2] D. P. DiVincenzo, Quantum Computation, Science 270 (1995) 255-261.

[3] L. M. K. Vandersypen, M. Steffen, G. Breyta, C. S. Yannoni, M. H. Sherwood, I. Chuang, Nature 414 (2001) 883-887.

[4] S. L. Braunstein, C. M. Caves, R. Jozsa, N. Linden, S. Popescu, R. Schack, Phys. Rev. Lett. 83 (1999) 1054-1057.

[5] W. S. Warren, Science 277 (1997) 1688-1690.

[6] URL: www.bruker.com/products/mr/epr/epr-resonators-acessories/epr-accessories/pulse-epr-accessories/spinjet-awg/overview.html.

[7] K. Sato, S. Nakazawa, R. Rahimi, T. Ise, S. Nishida, T. Yoshino, N.Mori, K. Toyota, D. Shiomi, Y. Yakiyama, Y. Morita, M. Kitagawa, K. Nakasuji, M. Nakahara, H. Hara, P. Carl, P. Hofer, T. Takui, Molecular electron-spin quantum computers and quantum information processing: pulse-based electron magnetic resonance spin technology applied to matter spin-qubits, J. Mater. Chem. 19 (2009) 3739-3754.

[8] F. Jelezko, T. Gaebel, I. Popa, M. Domhan, A. Gruber, J. Wrachtrup, Observation of coherent oscillation of a single nuclear spin and realization of a two-qubit conditional quantum gate, Phys. Rev. Lett. 93 (2004) 130501.

[9] S. Bertaina, S. Gambarelli, T. Mitra, B. Tsukerblat, A.Müller, B. Barbara, Quantum oscillations in a molecular magnet, Nature 453 (2008) 203-206.

[10] S. Bertaina, S. Gambarelli, A. Tkachuk, I. N. Kurkin, B. Malkin, A. Stepanov, B. Barbara, Rare-earth solid-state qubits, Nature Nanotechnology 2 (2007) 39-42.

[11] A. Abragam, B. Bleaney, Electron paramagnetic resonance of transition ions, Clarendon Press, Oxford, 1970.

[12] S. Bertaina, L. Chen, N. Groll, J. Van Tol, N. S. Dalal, I. Chiorescu, Multiphoton coherent manipulation in large-spin qubits, Phys. Rev. Lett. 102 (2009) 050501.

[13] S. Bertaina, M. Martens, M. Egels, D. Barakel, I. Chiorescu, Resonant single-photon and multiphoton coherent transitions in a detuned regime, Phys. Rev. B 92 (2015) 024408.

[14] H. A. Buckmaster, Y. H. Shing, A survey of the EPR spectra of Gd^{3+} in single crystals, Physica Stat. Sol. A 12 (1972) 325-361.

[15] C. F. Hempstead, K. D. Bowers, Paramagnetic resonance of impurities in $CaWO_4$. I. Two S-state ions, Phys. Rev. 118 (1960) 131-134.

[16] J. S. M. Harvey, H. Kiefte, Temperature dependence of the crystal-field splittings in Gd^{3+}:$CaWO_4$, Canadian J. Phys. 49 (1971) 995-1003.

[17] J. S. Thorp, G. Brown, H. P. Buckley, Dipolar line broadening in gadolinium-doped calcium tungstate, J. Materials Science 9 (1974) 1337-1343.

[18] J. S. Thorp, E. A. E. Ammar, Site occupation in gadolinium-doped calcium tungstate, J. Materials Science 14 (1979) 401-406.

[19] V. A. Vazhenin, V. B. Guseva, M. Yu. Artemov, Effects of averaging of spin packets of interacting resonances in Gd^{3+} EPR spectra of scheelites, Physics of the Solid State 45 (2003) 2271-2275.

[20] J. S. Thorp, E. A. E. Ammar, Spin-lattice relaxation in gadolinium-doped calcium tungstate, J. Materials Science 11 (1976) 1215-1219.

[21] J. R. Klauder, P. W. Anderson, Spectral diffusion decay in spin resonance experiments, Phys. Rev. 125 (1962) 912-932.

[22] K. M. Salikhov, S. A. Dzuba, A. M. Raitsimring, The theory of electron spin-echo signal decay resulting from dipole-dipole interactions between paramagnetic centers in solids, J. Magn. Res. 42 (1981) 255-276.

[23] W.B. Mims, Phase memory in electron spin echoes, lattice relaxation effects in $CaWO_4$: Er, Ce, Mn, Phys. Rev. 168 (1968) 370-389.

[24] E. Baibekov, I. Kurkin, M. Gafurov, B. Endeward, R. Rakhmatullin, G. Mamin, Coherence times and Rabi oscillations in $CaWO_4$: Cr^{5+} crystal, J. Magn. Res. 209 (2011) 61-68.

[25] E. I. Baibekov, M. R. Gafurov, D. G. Zverev, I. N. Kurkin, B. Z. Malkin, B. Barbara, Coherent manipulation of dipolar coupled spins in an anisotropic environment, Phys. Rev. B 90 (2014) 174402.

[26] E. I. Baibekov, Decay of Rabi oscillations induced by magnetic dipole interactions in dilute paramagnetic solids, JETP Letters 93 (2011) 292-297.

[27] S. Wimperis, Broadband, narrowband, and passband composite pulses for use in advanced NMR experiments, J. Magn. Res. 109 (1994) 221-231

[28] J. J. L. Morton, A. M. Tyryshkin, A. Ardavan, K. Porfyrakis, S. A. Lyon, G. A. Briggs, High fidelity single qubit operations using pulsed electron paramagnetic resonance, Phys. Rev. Lett. 95 (2005) 200501

[29] I. K. Ishmuratov, E. I. Baibekov, Bulk quantum computation with pulsed electron paramagnetic resonance: simulations of single-qubit error correction schemes, J. Low Temp. Phys. DOI: 10.1007/s10909-015-1411-x.